# Versatile transmission/reflection tomographic diffractive microscopy approach

Ludovic Foucault, Nicolas Verrier, Matthieu Debailleul, Jean-Baptiste Courbot, Bruno Colicchio, Bertrand Simon, Laurent Vonna, Olivier Haeberle

# A versatile transmission/reflection tomographic diffractive microscopy approach

LUDOVIC FOUCAULT,[1] NICOLAS VERRIER,[1] MATTHIEU DEBAILLEUL,[1] JEAN-BAPTISTE COURBOT,[1] BRUNO COLICCHIO,[1] BERTRAND SIMON,[2] LAURENT VONNA,[3] AND OLIVIER HAEBERLÉ[1,*]

[1] *Institut de Recherche en Informatique, Mathématiques, Automatique et Signal (IRIMAS EA7499), Université de Haute-Alsace, 61 rue Albert Camus, 68093 Mulhouse Cedex, France*
[2] *Laboratoire Photonique Numérique et Nanoscience (LP2N), Université de Bordeaux, Institut d'Optique Graduate School, CNRS-UMR 5298, Talence 33405, France*
[3] *Institut de Science des Matériaux de Mulhouse (IS2M), Université de Haute-Alsace, CNRS-UMR 7361, 15 rue Jean Starcky, 68057, Mulhouse, France*
[*] *olivier.haeberle@uha.fr*

**Abstract:** Tomographic diffractive microscopy (TDM) has gained interest in recent years, thanks to its ability at delivering high-resolution, three-dimensional images of unlabelled sample. It has been applied to transparent samples, in transmission mode, as well as to surfaces studies, in reflection mode. Mudry *et al.* [Opt. Lett. 35, p. 1857(2010)] introduced in 2010 the concept of mirror-assisted tomographic diffractive microscopy (MA-TDM), an elegant approach for achieving quasi isotropic-resolution microscopic imaging, but which still is to be experimentally applied. In this work, we show that a simplified version of MA-TDM allows for transforming a reflective TDM set-up into a more versatile instrument, also capable of observing transparent samples in transmission mode, if using specific sample holders, made out of a mirror, coated with a low-thickness transparent spacer.



## 1. Introduction

Tomographic diffractive microscopy (TDM) [1] has been actively developed in recent years, and has proven being able to deliver high-resolution images of unlabeled samples [2,3]. The technique works in transmission as well as in reflection modes, and commercial implementations are even now available for transmission TDM, which is well adapted for investigations on biological samples (for recent reviews about the technique, see for example [4,5]).

Most TDM systems are based on holographic recording of diffraction patterns to acquire information about the sample, combined with angular scanning of the illumination to perform tomographic acquisitions. A numerical inversion model is then used to compute the image of the observed specimen. In its simplest versions, first Born approximation can be used [6], performing reconstructions via 2-D and 3-D Fourier transforms, which have the advantage of ease of use and speed of reconstruction [7]. Rotation of the sample has also been successfully implemented to obtain more accurate images [8–12]. Combining both approaches is also possible [13], which permits, in its optimal configuration, to deliver sample's 3-D images with improved *and* isotropic resolution [14]. An alternate to obtain almost isotropic-resolution images is 4Pi tomography, proposed in 2002 by Lauer [15], but this method is yet to be experimentally implemented.

Besides these achievements, specific developments to simplify and/or speed-up data acquisitions have also been performed [16–24]. In this work, we propose an approach for simplifying so-called mirror-assisted tomography, which was introduced by Mudry *et al.* in 2010 [25]. We show that, at the price of having to use specific sample holders, this approach would allow for performing transmission or reflection TDM acquisitions using the same microscope set-up, thus widening the interest for this technique.

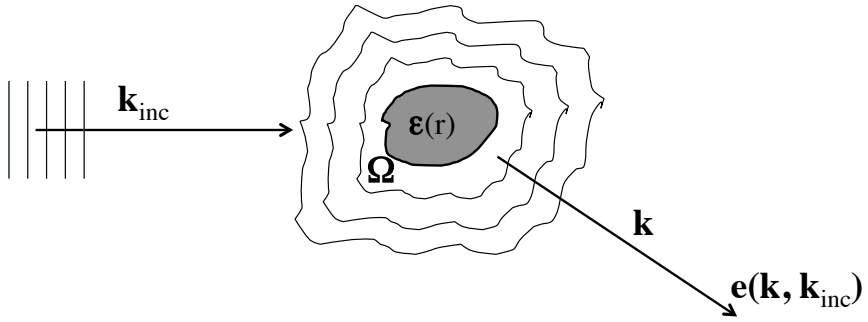


Fig. 1. A plane wave depicted by its wavevector $\mathbf{k}_{inc}$ illuminates an object, bounded on support $\Omega$ characterized by its relative permittivity $\epsilon(r)$. The diffracted field is decomposed into a sum of plane waves of wavevectors **k.**

## 2. Basics of TDM

Tomographic diffractive microscopy in transmission is under development by several groups worldwide, and has already been used to study a wide variety of biological samples [3–5,16,26–37], only making use of the intrinsic index contrasts of the sample.

We here briefly describe the link between the observed sample's refractive index three-dimensional distribution and the measurement of the field (in phase and amplitude) it diffracts when illuminated by a plane wave. We limit the description to scalar approximation for the sake of simplicity. Lauer [15] proposed an extension to account for the vectorial nature of the light, to which the interested reader is referred, as well as to review papers about the technique [1,4].

So, one considers a scalar monochromatic plane wave of wavelength $\lambda = 2\pi c/\omega$, emitted by a source S(**r**), and illuminating a transparent object, characterized by its relative permittivity $\epsilon(r)$ (see Fig. 1). When omitting the $\exp(-i\omega t)$ time dependence for simplicity, the Helmholtz equation simply writes as:

$$\Delta E(\mathbf{r}) + k_0^2 E(\mathbf{r}) = \chi(\mathbf{r}) k_0^2 E(\mathbf{r}) + S(\mathbf{r}) \tag{1}$$

with $k_0 = 2\pi/\lambda$ the wavevector, and with $\chi = 1 - \epsilon$ the contrast of permittivity. Then, one makes use of the Green's function:

$$G(\mathbf{r}) = -\exp(ik_0\mathbf{r})/4\pi r \tag{2}$$

to rewrite an integral equation for the total field:

$$E(\mathbf{r}) = E_{inc}(\mathbf{r}) + k_0^2 \int G(\mathbf{r} - \mathbf{r}')\chi(\mathbf{r}')E(\mathbf{r}')d(\mathbf{r}') \tag{3}$$

to be calculated over the support of the object $\Omega$, and in which $E_{inc}$ depicts the incident field emitted by the source S(r). In transmission microscopy, one considers only the far-field. For an observation point r which is located far from the object, for any r' in $\Omega$, one has $r'^2/\lambda \ll r$. As a consequence, one can simplify the diffracted field:

$$E_d(\mathbf{r}) = -\frac{\exp(ik_0 r)}{4\pi r} e(\mathbf{k}), \tag{4}$$

and write the amplitude of the scattered field $e(\mathbf{k})$ as:

$$e(\mathbf{k}) = k_0^2 \int \exp(-i\mathbf{k}.\mathbf{r}')\chi(\mathbf{r}')E(\mathbf{r}')d(\mathbf{r}') \tag{5}$$

In the following, the incident field is considered for simplification to be a plane wave, with wavevector $\mathbf{k}_{inc}$, so written as $E_{inc}(r) = A_{inc} \exp(i\mathbf{k}_{inc}.\mathbf{r})$. Also for the sake of simplicity, we restrict here the analysis to weakly diffracting objects, so that the first Born approximation remains valid. Under these assumptions, one can then write:

$$e(\mathbf{k}, \mathbf{k}_{inc}) \propto C\tilde{\chi}(\mathbf{k} - \mathbf{k}_{inc}) \tag{6}$$

with $C = 8\pi^3 A_{inc} k_0^2$. Equation (6) links Fourier coefficients of the relative permittivity of the object with the amplitude of the far-field it diffracts when illuminated by a plane wave [6].

Because only elastic scattering is considered, diffracted vectors $\mathbf{k}_{diff}$ have same amplitude as $\mathbf{k}_{inc}$, thanks to energy conservation. The ensemble of $\mathbf{k}_{diff}$ then depicts the so-called Ewald sphere. Then from the elastic scattering condition, this set of diffracted $\mathbf{k}_{diff}$ vectors transforms into object ($\mathbf{k}_o$ vectors, via a simple translation:

$$\mathbf{k}_o = \mathbf{k}_{diff} - \mathbf{k}_{inc} \tag{7}$$

### 2.1. Transmission TDM

In practice, one has to separately consider two cases: one half of the Ewald sphere comprises $\mathbf{k}_{diff}$ vectors propagating in same direction as incident illumination $\mathbf{k}_{inc}$, to form an image in transmission microscopy, while the second half contains those wavevectors forming an image in reflection microscopy (next section). Furthermore, only a portion of the half Ewald sphere in transmission can be captured in practice, because of the limited numerical aperture of the detection objective.

Following this framework, Figure 2 describes information acquisition for Digital Holographic Microscopy (DHM) (Fig. 2(a)), and for TDM with illumination rotation (Figs. 2(b)). For the sake of simplicity, in this work Optical Transfer Functions (OTFs) are displayed in 2-D views, their 3-D shapes being obtained by rotation around the optical axis ($k_z$-axis). Complete, 3-D representations with animations describing their construction are available in the supplementary materials of Ref. [14]. Figure 2(a) explains that, for transparent objects, DHM has good lateral resolution, thanks to wide $\mathbf{k}_x, \mathbf{k}_y$ extension of the $\mathbf{k}_o$ vector set, but bad resolution along the optical axis, because of its narrow extension along the $\mathbf{k}_z$ axis [2]. When the illumination is tilted as in Fig. 2(b), one can capture different information about the sample. And finally, for a large number of illuminations (Fig. 2(c)), synthesizing a high-numerical aperture condenser permits, by accumulating information in Fourier space, to obtain an expanded and filled $\mathbf{k}_o$ set, namely the OTF of the system, with a so-called "doughnut shape", characteristic of transmission microscopy [38]. The presence of a so-called "missing-cone" of unrecorded frequencies explains the low sectioning capabilities of transmission microscopes, including tomographic microscopes [2]. When numerical apertures at illumination and at detection are different, the support becomes asymmetric [38]. This filled and extended frequency support leads to the doubled lateral resolution of TDM compared to DHM [15], experimentally reaching resolution near or even better than 100 nm [2, 3].

Beside improved resolution, a second characteristic feature of TDM is its capability to clearly distinguish refractive and absorptive structures within the observed specimen [2, 15, 39–42]. Commercial systems are now available [43, 44].

### 2.2. Reflection TDM

The case of TDM in reflection [45–48] can be directly understood using same framework. As in transmission configuration, Fourier components of the diffracted waves that can be collected are limited by the numerical aperture of the microscope objective, the difference in resulting object components, which are captured, coming from the different translation of vector $-\mathbf{k}_i$ in reflection configuration, compared to transmission case. In reflection, the reconstructed object frequencies

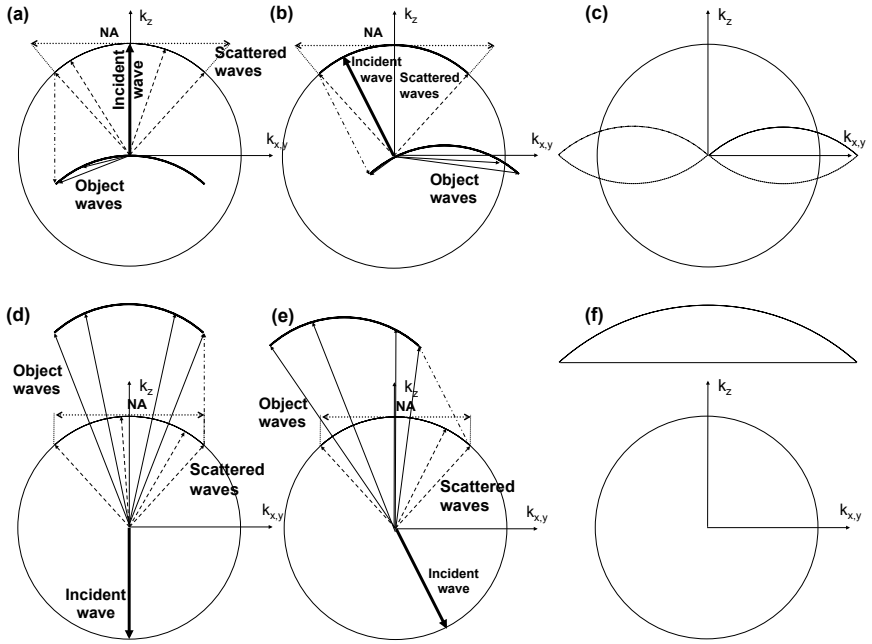


Fig. 2. Principle of TDM: construction of the Optical Transfer Function, in transmission (a-c) and reflection (d-f) configurations. (a,d): conventional holographic microscopy with illumination along the optical axis. (b,d): with inclined illumination, (e,f): OTF support with full angular scanning.

cap of sphere is shifted towards higher frequencies along the optical axis, Fig. 2(d) (the translation vector being the opposite as in transmission mode), while in transmission holography, the object cap of sphere has its summit at the frequency origin, see Fig. 2(a).

As seen before, another object frequency set become recordable when changing the angle of illumination, thanks to the different translation to be done, as illustrated by Fig. 2(e) . For the transmission case, the captured object frequency cap of sphere passes again through the origin of frequencies (Fig. 2(b)), while in reflection case, the same point from the diffracted frequencies cap of sphere ends up located along $\mathbf{k}_z$ axis, but at $k_z > 0$ (Fig. 2(e)).

Again, for a large number of incidences, the synthetic aperture process allows for constructing an extended and filled support of object frequencies, depicting a portion of a ball, with same lateral extension as in transmission case, but now comprising high frequencies along the optical axis, depicted in Fig. 2(f). This simplified approach already permits to double the lateral resolution compared to conventional holography in reflection [45–50], and to improve the optical sectioning properties [49], as well as profile reconstructions in profilometry [50]. When considering highly-scattering specimens for which multiple diffraction occurs, and solving the full electromagnetic inverse problem, true superresolution is even possible [51].

## 3. Isotropic-resolution TDM

While TDM with illumination rotation has already proven to be a very useful instrument, especially for biological investigations, its imaging capabilities are affected by the “missing cone”, inducing poor optical sectioning, if simpler numerical methods based on the Born or Rytov approximations are used. When more elaborate reconstruction methods are used, and/or if a priori knowledge about the sample is injected, which permits to numerically fill the missing cone, image quality is well improved. However, the final images are anyway characterized by a

strong anisotropic resolution: it is an inevitable consequence of the transmission OTF, which is much wider along x-y directions than along the optical axis z. Several approaches have therefore been examined to provide isotropic-resolution images.

The first one considers rotating the sample.This method permits to obtain a quasi-completely filled ball as final OTF (see Fig. 3(a), but because of the initial cap of sphere curvature, a so-called "missing apple-core" remains along the sample rotation axis, here the x-axis [52]. A solution to completely fill the OTF could then consist in performing another rotation of the sample around a second axis, perpendicular to the first one [13, 52]. This approach presents however drawbacks. Performing a precise sample rotation at microscopic scale, and compatible with interferometric measurements can be difficult. A large number of rotations is necessary for accurate reconstructions. Finally, the OTF maximal extension is smaller than maximal achievable extension in TDM with illumination rotation [53].

A second approach to obtain an improved- and isotropic resolution associates illumination rotation and specimen rotation [53], with the advantage, compared to the previous one, that merging several doughnuts from TDM with illumination rotation to obtain a quasi-spherical, extended final OTF, now only requires a few precise sample rotations. Figure 3(b) illustrates this advantage, displaying the OTF obtained when merging 4 doughnuts. However, this method obviously also necessitates to precisely control the rotation of a microscopic sample [14].

Lauer [15] has proposed another possible approach: combining transmission and reflection acquisitions in a 4-Pi TDM setup. As in fluorescence microscopy [54], the use of two opposing microscope objectives must permit to collect the transmitted part as well as the retrodiffracted part of the scattered wave, when illuminating the sample through the first objective. Then, switching the illumination objective would allow for collecting a second transmitted spectrum, which appears to superimpose with the first one, but also a second retrodiffracted part, which complement the previously acquired ones [15]. Figure 3(c) shows the combined 4Pi-OTF resulting from merging two transmission TDM OTFs (which superimpose) and two opposite reflection TDM OTFs. In this configuration, longitudinal resolution is even slightly better than the lateral one, because of the limited numerical aperture of the collecting objectives [54].

The main difference resides in the sequential approach: in fluorescence 4Pi microscopy, illumination has to be made through both objectives at the same time, while fluorescence signal has to be collected simultaneously by both objectives and must interfere onto the detector to reach the highest resolution (4Pi Type C [54]). The difficulty of adjusting the interferometer (the coherence length in fluorescence being very short, in the few $\mu$m range [55]) probably explains that this powerful technique has not attracted a wider interest. Furthermore, the specimen is to be observed sandwitched between two cover glasses, which may add additional difficulties in sample preparation and manipulation.

One advantage of 4Pi TDM, compared to fluorescence 4Pi microscopy, is that the coherence length of the illumination would greatly leverage the constraints on the interferometers' arms length. One could even slightly reduce the setup's complexity by having only three interferometers, as the transmitted parts are redundant. But the system would anyway be way more complex than current TDM implementations in either transmission or reflection. Another predictable difficulty is the necessity to register the data in Fourier space, which in 4Pi TDM have to be acquired sequentially by different experiments in transmission and reflection, onto different detectors. If the numerical aperture is high enough (NA>1.45 for oil immersion objectives), superimposition zones would indeed exist in Fourier space, which could be used to renormalize the data [15], but not for water immersion objectives (NA=1.2) or standard oil immersion objective (NA=1.4). So, imaging performances of 4Pi TDM have not yet been experimentally explored up to know.

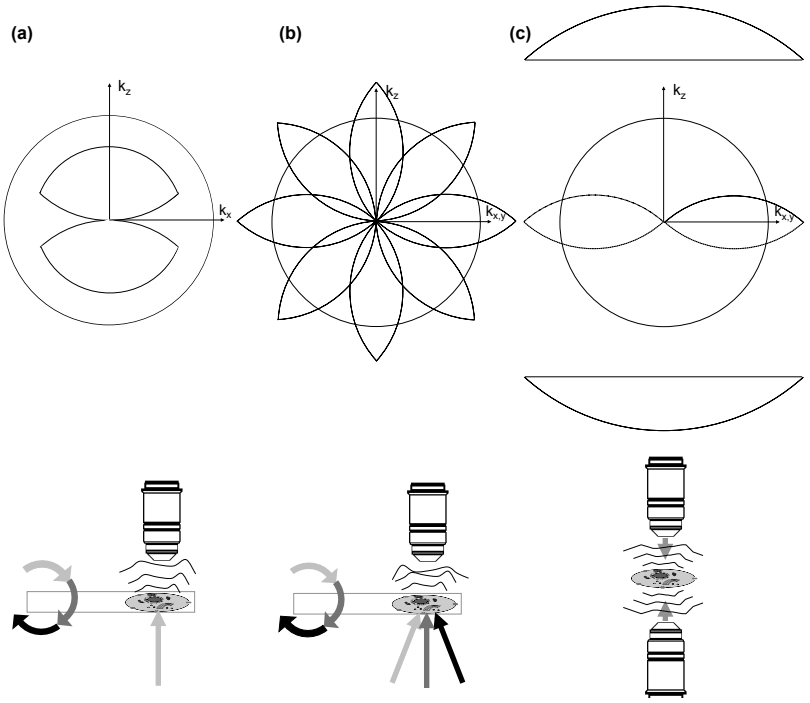


Fig. 3. Optical Transfer Function for conventional approaches for isotropic-resolution TDM. (a): SR-TDM with specimen rotation: sample is rotated in a conventional holographic microscope. (b): IRSR-TDM: combined approaches with sample rotated in an IR-TDM using illumination rotation. (c): 4Pi TDM, combining transmission and reflection TDM in a dual-objective setup.

## 4. Mirror-Assisted TDM as versatile transmission/reflection TDM

### *4.1. Conventional Mirror-Assisted TDM*

In order to facilitate label-free samples with isotropic resolution, Mudry *et al.* [25] introduced in 2010 the concept of mirror-assisted reflection optical diffraction tomography. The configuration is similar to that of a standard reflection TDM, except that the sample has to be placed in the vicinity of a mirror. The important point in the inversion procedure is to properly account for this mirror. Mudry *et al.* [25], solving the electromagnetic problem, showed that the solution is directly related to Born solution, making use of cosine transforms instead of Fourier transforms. With numerical simulations, they then explored the concept and its imaging performances. This elegant approach has however not yet been experimentally demonstrated.

Such a configuration achieves in fact 4Pi detection, but using only one objective, by clever use of the mirroring effects, which plays the role of the second objective. A qualitative explanation can be given in the framework of weakly diffractive samples. Figure 4(a) illustrates the concept. When the sample is placed near a perfectly reflecting mirror, slightly above it, and observed using a reflection TDM, one can consider (for weakly diffracting samples) that it is illuminated by two waves. First, the one emerging from the objective and illuminating the sample (grey arrow), and being diffracted by it. Then, its non diffracted part (within first Born approximation, it corresponds to the illumination wave) is reflected by the mirror (black arrow), and illuminates again the sample.

If one now considers the diffracted components, following situation arises. The front wave diffracted by the original impinging illumination comprises a forward-scattered part, and a

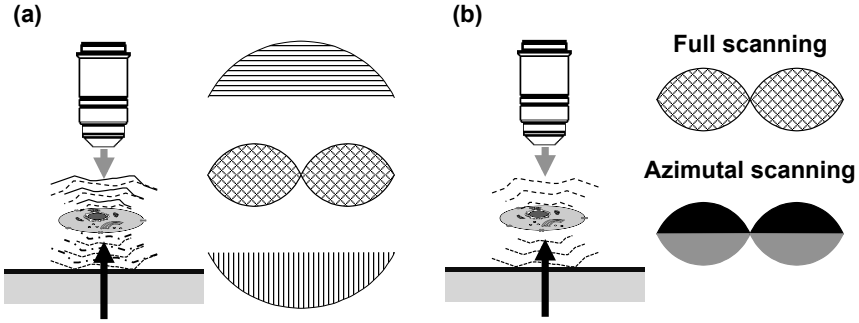


Fig. 4. Principle of mirror-assisted TDM: construction of the OTF (a): standard configuration, acting as a 4Pi TDM. (b): simplified version when backward-scattering from the sample is negligeable, acting as a dual view transmission TDM, with full- or azimuthal-only angular scannning.

backward-scattered one. The latter (Original Illumination-Backward Scattered Wave or OI-BSW: plain line in Fig. 4(a)) is captured by the objective, as in a reflection TDM. When angular scanning is applied, the upper cap of ball is captured (horizontal stripes on the upper part of the OTF). The forward-scattered wave (OI-FSW: dotted line) is then reflected by the mirror, to be finally captured by the objective. When angular scanning is applied, the central doughnut is captured (+45° stripes in the central part of the OTF). Same description applies to the second illuminating wave, reflected by the mirror. When diffracted, its forward-scattered part (Reflected Illumination-Forward Scattered Waved or RI-FSW: dashed line) is directly captured by the objective, and angular scanning is applied, a second, superimposed central doughnut is captured (-45° stripes). Simultaneously, its backward-scattered part (Reflected Illumination-Backward Scattered Wave or RI-BSW: dotted-dashed line) propagates towards the mirror, is reflected, then propagates towards the objective. When angular scanning is applied, the lower cap of ball is captured (vertical stripes in the lower part of the OTF). Finally, same OTF is obtained as in a conventional, two-objective 4Pi TDM system [15, 25].

### *4.2. Simplified Mirror-Assisted TDM*

The above-described configuration can be simplified, if one considers rather large (several wavelength), highly transparent samples, with index of refraction distribution values remaining very close to that of the surrounding medium. For such samples in fact, diffraction mostly propagates in the forward direction, and the retrodiffracted component is often negligible. For example, reflection coefficients for glass (n=1.525) to oil (n=1.515) interface at 45° incidence are equal to $4.10^{-5}$ and $2.10^{-9}$ in s- and p-polarization, respectively [56]. Similarly, 5$\mu$m diameter glass sphere in oil as a backscattering efficiency of about $4.10^{-5}$ (see e.g. [57]).

So, for those samples for which the retrodiffracted components are negligible with respect to the forward-scattered ones, Fig. 4(a) simplifies into Fig. 4(b): a mirror-assisted tomographic diffractive microscope then transforms into a dual-view transmission TDM. When full angular scanning is used, one finally captures twice the central doughnut of a transmission microscope, the mirroring effect simply resulting into a duplicate image of the specimen. Contrary to a regular 4Pi or mirror-assisted TDM, there is no gain in longitudinal resolution, but it may anyway have interesting consequences for building a TDM experiment: it shows that a reflection TDM can be turned into a transmission TDM. This comes at the price that special sample supports are to be used, but would transform a purely reflection TDM into a more versatile system, able to observe surfaces of reflecting samples, as well as transparent samples, such as those often encountered

in biology (individual cells such are red or white blood cells, but also isolated, cultured cells, pollens, spores, diatoms, radiolaria. . . ).

Such mirror-assisted configuration can also help addressing another practical limitation of some conventional transmission TDM systems. Because TDM is inherently a sequential system, acquiring data one illumination angle to the next can be time-consuming. In order to diminish the number of holograms to be taken, and therefore to accelerate acquisitions, the following assumption can be done. When the observed sample does not present absorption, its Fourier spectrum obeys Hermitian symmetry. As a consequence, full angular scanning is not necessary to acquire a complete spectrum. Indeed, an azimuthal-only scanning, performed at maximum illumination inclination (Fig. 2(c)), allows for acquiring the upper half-spectrum (with positive $k_z$ components) in transmission microscopy [17, 38]. Then, applying Hermitian symmetry permits to reconstruct the lower half-spectrum [58]. However, this approach may induce reconstruction artifacts: for example, if the observed sample does present some absorptive sub-structures, then, they will be simply erased when applying Hermitian symmetry. Conversely, if not applying Hermitian symmetry, Fourier transforming an asymmetric data support (only half a doughnut is recorded) will make falsely appear structures in the imaginary part of the reconstructed image, namely absorptive structures, in a non-absorbing sample. Similarly, absorbing structures may be falsely reconstructed as refractive ones.

Mirror-assisted TDM, using only azimuthal scanning, permits to record both halves of the doughnut as depicted in Fig. 4(c), thanks to the duplicated illumination. The system acts then as two transmission TDM, both using azimuthal illumination and observing same sample, but from opposite sides. The reflected illumination (black arrow) gives rise to the upper half-doughnut (with positive $k_z$ components), as in a conventional transmission TDM used with azimuthal illumination at maximum angle (Fig. 2(c)). The original illumination (grey arrow) yields the lower half-doughnut (with negative $k_z$ components), as in a conventional transmission TDM used with azimuthal illumination at maximum angle, but looking at the sample from the other side. Both recorded half doughnuts complement in this configuration, to form the complete support of a transmission TDM with full angular scanning. As a consequence, no assumption about sample being non-absorptive is necessary for its numerical reconstruction. However, because both half doughnuts are acquired simultaneously, they are intermixed in the successive acquired interferograms, so that a proper demodulation scheme is to be applied for sample image reconstruction.

### *4.3. Simulations*

Figure 5 illustrates these properties of simplified mirror-assisted TDM. A synthetic object with compound (refraction and absorption) refractive properties is considered, depicted on Fig. 5(a). For this simulation, following parameters are considered: 100x objective with numerical aperture NA = 1.4 and illumination at 475 nm. The object size is 11.5 $\mu$m x 10$\mu$m, and the object is considered being placed 5$\mu$m above a perfectly reflective mirror (located in the middle of the numerical volume). Figure 5(b) shows the simulated images, which would be obtained in a mirror-assisted TDM with full angular scanning, taking into account the mirroring effect, and reconstructing the images assuming a simple transmission TDM. The twin-images are deformed by the limited bandwidth of the acquisition system, especially along the vertical (optical) axis, because of the missing cone. Twin-images are however identical, both in real- and imaginary part, simply illustrating the duplication of the observed sample by the mirror.

Figure 5(c) shows the simulated images with azimuthal-only angular scanning, taking into account the mirroring effect, and reconstructing the images assuming a simple transmission TDM. Note that after reconstruction, the twin-images are not identical anymore. Furthermore, one can notice in the real part, as well as in the imaginary part, that structures originating from both components of the original compound object are mixed. These are direct consequences of the

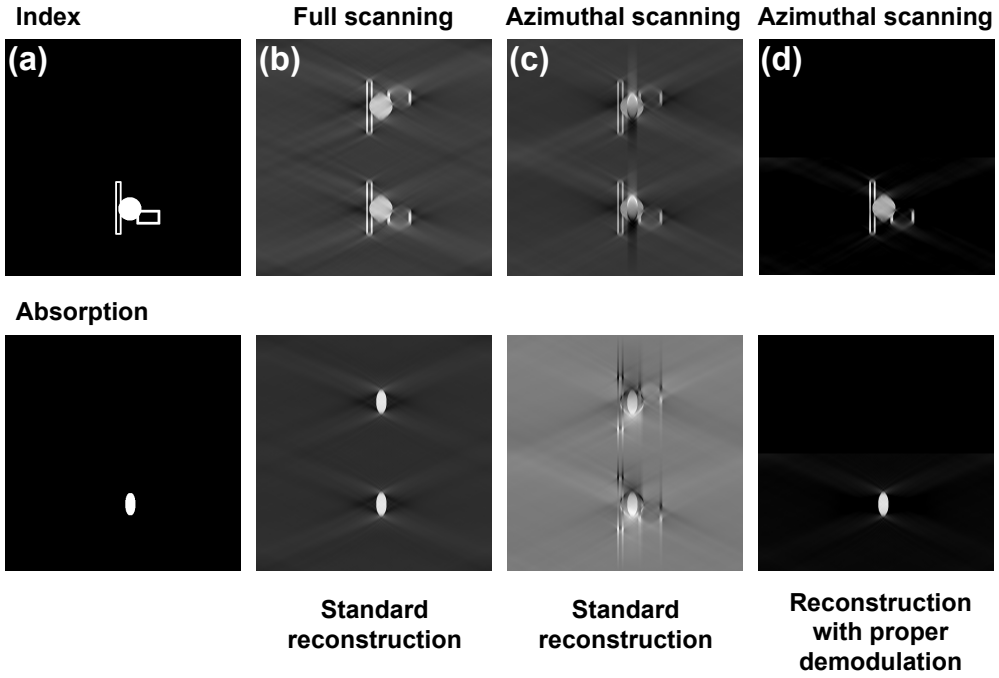


Fig. 5. Simulation of simplified mirror-assisted tomography. (a): initial object. (b): reconstruction as in a conventional transmission TDM, taking into account the mirroring effect, and with full illumination scanning. (c): same as (b), but with azimuthal illumination scanning. (d): with adapted data demondulation before reconstruction.

symmetry-braking of the problem induced by a incomplete scanning resulting in an asymmetric OTF, if one does not properly unmix the information.

An adapted demodulation is therefore necessary to correctly reassign information. Taking into account the characteristics of the system, based on duplicating images by the mirror, the following scheme is derived.

If acquiring data using full angular scanning, simply reconstruct twin-images as if a regular transmission TDM had been used. Split the image along the symmetry plane so as to isolate a unique image of the observed sample: Fig. 5(b).

If acquiring data using azimuthal-only angular scanning, following procedure can then be applied, illustrated in Fig 6:

- reconstruct twin-images as if a regular transmission TDM had been used;
- split the (complex) image along the symmetry plane to separate images of the object and its reflection in the mirror;
- Fourier transform each image;
- vertically flip the spectrum of the reflection image;
- add both spectra to reconstitute the full doughnut of a transmission TDM with full angular scanning;
- reconstruct final refraction and absorption images of the sample;

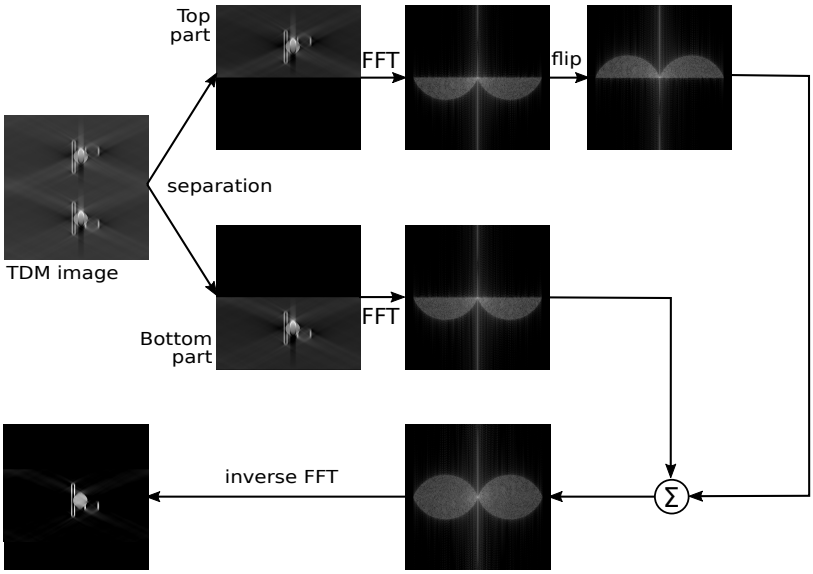


Fig. 6. Demodulation of the images obtained from simplified mirror-assisted TDM, to cancel the mirroring effect and properly reassign information relative to the real (index) and imaginary (absorption) contributions.

Figure 5(d) illustrates this adapted demodulation process. Note that this final image, while using azimuthal-only angular scanning data, now properly reassigns real (index) and imaginary (absorption) contributions, while at the same time canceling the mirroring effect to reconstruct a single object without its twin image.

### *4.4. Preliminary experimental results*

We performed experiments to validate this simplified mirror-assisted TDM approach. Figure 7 illustrates the mirroring effect. Small, quasi-flat microcrystals have been deposited onto a specially prepared glass slide, vacuum-coated with aluminum for the reflection function of the mirroring effect, then spin-coated with a 6 $\mu$m thickness transparent polystyrene layer, and observed using our reflection TDM system [49, 50] using a 100x, N.A. = 1.4 objective, and illumination at 475 nm. Microcrystals are embedded in Eukitt as mounting medium. Data have been acquired with full-angular scanning, and then processed as if resulting from our transmission TDM [7].

Figure 7(a) depicts the en-face view of the 3-D reconstruction volume, while Figs. 7(b,c) show same data cube, rotated by 45° and 90°, respectively. As expected, the mirroring effect duplicates the image of the observed sample. As described in previous section, in order to isolate a single image of the observed sample, one can simply split the reconstructed volume along the mirror plane, indicated by white arrows on Fig. 7(c). However, this configuration requires full angular scanning of the illumination, so it does not provide gain in speed of acquisition and amount of data to be processed.

Figures 7(d,e) show two phase images (demodulated holograms) of a 6 $\mu$m diameter polystyrene bead, located 6 $\mu$m above a gold reflective layer, and illuminated at 532 nm, at high incidence angle and for two different azimuthal angles. Beads are embedded in Eukitt as mounting medium.Note the elongated aspect of the bead, due to the inclined illumination, as well as the reflection of the bead in the mirror, observed spatially separated, thanks to the high angle of incidence illumination. The reflection of the bead in the mirror appears rotating around the direct

view of the bead (See also Visualization 1).

Figure 7(f) depicts the direct reconstruction, assuming a transmission microscope had been used, and for azimuthal illumination only (contrary to Figs. 7(a-c) obtained with full angular scanning). Note that the reflected image (upper part of the image) is of lower quality than the direct view (lower part of the image), indicating that the mirroring effect is not perfect. Nevertheless, this results validate the approach for azimuthal-only scanning, and that simple reconstructions based on the limited-validity Born approximation are morphologically correct. Figure 7(g) shows the reconstruction taking into account the mirroring effect: a single bead is reconstructed.

Figure 7(h) shows relative (compared to Eukitt) index of refraction profiles along the bead diameter, for the direct reconstruction from Fig. 7(h) and from Fig. 7(g) . Note that the bead diameter is correctly reconstructed, and that the profile from the demodulated bead (narrow-dashed line) is closer to the theoretical profile (solid line) than the profiles from the direct reconstruction (dotted line for the direct view of the bead, wide-dashed line for the reflected view of the bead), even in these unfavourable conditions. It however also confirms that more accurate reconstruction methods, finely taking into account the actual characteristics of the mirror, should be used in order to get higher precision reconstructions.

One can also point out some experimental restrictions of the approach. Within this framework, observed samples must indeed be (very) weakly absorptive/diffractive, so that those two diffracted waves OI-FSW and RI-BSW, which are retroreflected by the mirror, can be considered as primarily not being affected again by the sample, when they traverse it back, exactly like the illumination wave is considered as unperturbed in Born approximation. This is a limitation of the approach.

Sample dimensions are also to be taken into consideration for optimal observations. The mirror-assisted TDM concept requires the sample to be located not in contact with, but at a small distance from the mirror [25]. The thickness of the layer separating the sample from the mirror then has to be adapted. If too small, blurring of the twin images along the optical axis will mix them (because of the missing cone), at least partially, preventing their separation for reconstruction. If too large, limited depth of field will make it impossible to precisely record images of the sample and its reflection in the mirror. So, flatter objects, such as those presented in Fig. 7 are to be preferred for accurate reconstructions, at least when using simplest reconstruction methods based on Born or Rytov approximations.

These first results need to be confirmed for a larger class of objects, and elaborating more advanced reconstruction methods, but do validate the mirror-assisted TDM concept proposed by Mudry *et al.* [25] as well as the simplified approach we propose for transforming a reflection TDM into a more versatile instrument, by preparing highly transparent samples on special supports.

## 5. Conclusion and perspectives

We have studied a derivative of mirror-assisted tomography, initially proposed by Mudry *et al.* [25]. For samples, which mainly exhibit forward scattering, one can therefore neglect backward-scattered contributions, and in that case, a mirror-assisted tomographic microscope simplifies into a dual-view transmission microscope. As a consequence, a TDM system built for reflection microscopy can be used as a transmission TDM, constituting a versatile system, capable of observing surfaces of reflecting samples, as well as transparent samples. To do so, one has to use special sample supports, consisting in a reflective layer covered by a transparent layer to have the observed sample placed above the mirror, and not in contact with it [25].

The first experimental results presented in this paper confirm the validity of the approach. While working for very basic samples, the simplified demodulation method we propose here, taking benefit of the symmetries induced by the mirroring effect (and formally fully equivalent to the cosine transforms used in the seminal paper about mirror-assisted tomography by Mudry *et al.* [25]), are however to be improved for optimal image reconstructions. In particular, the

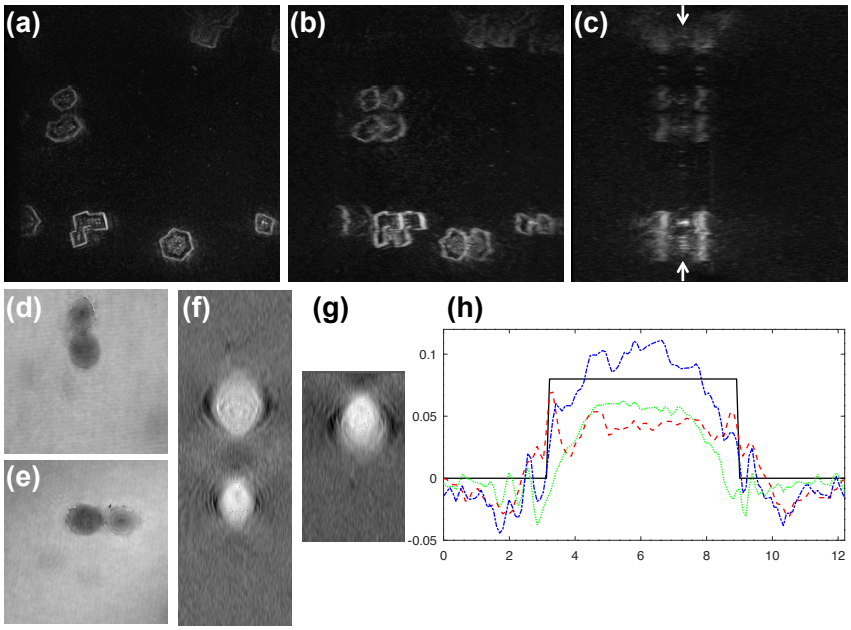


Fig. 7. Images obtained in a simplified mirror-assisted TDM. (a-c): using a reflection TDM system (here with full angular scanning) in conjunction with special sample supports, direct reconstruction as in Fig. 5(b) makes transparent microscrystals appear twinned, but as observed in a transmission TDM system. (d-e): illustration of the mirroring effect with a polystyrene bead illuminated at high incidence. (f,g): bead reconstructions assuming direct reconstruction (f) as in Fig. 5(b), and with proper demodulation (g) correcting for the mirroring effect. (h): reconstruction profiles of the index of refraction variations compared to the theoretical profile.

image reconstruction process here assumes that a perfect mirror is used. In practice, for obtaining highest-resolution images, one has indeed to use short wavelength illumination [3], for which reflective surfaces may not be anymore considered as perfect, as well as high numerical apertures, at detection but also at illumination [2, 3], conditions inducing non negligible polarization effects when reflection occurs.

To the best of our knowledge, such experimental conditions (rather large, three-dimensional samples a few tens of micrometers in size, and high numerical aperture illumination and detection in a reflection set-up) have not yet been treated in the literature of TDM, but Godavarty *et al.*'s work [59] could constitute a good starting point to expand the domain of use of mirror-assisted tomographic diffractive microscopy [25]).

## Acknowledgements

We acknowledge financial support from Région Grand Est for L. Foucault PhD fellowship under grant n◦ 544/15/C13 and Agence Nationale de la Recherche (ANR) (ANR-11-JS10-0003 OSIRIS). We would like to thank P. C. Chaumet, H. Giovaninni, G. Maire and A. Sentenac for enlightening discussions about Mie diffraction and mirror-assisted tomography.

## Founding

Région Grand-Est (544/15/C13); Agence Nationale de la Recherche (ANR) (ANR-11-JS10-0003 OSIRIS).

## References


1. O. Haeberlé, K. Belkebir, H. Giovaninni, and A. Sentenac, "Tomographic diffractive microscopy: basics, techniques and perspectives," J. Mod. Opt. **57**, 686–699 (2010).
2. M. Debailleul, V. Georges, B. Simon, R. Morin, and O. Haeberlé, "High-resolution three-dimensional tomographic diffractive microscopy of transparent inorganic and biological samples," Opt. Lett. **34**, 79–81 (2009).
3. Y. Cotte, F. Toy, P. Jourdain, N. Pavillon, D. Boss, P. Magistretti, P. Marquet, and C. Depeursinge, "Marker-free phase nanoscopy," Nat. Photonics **7**, 113 (2013).
4. D. Jin, R. Zhou, Z. Yaqoob, and P. T. C. So, "Tomographic phase microscopy: principles and applications in bioimaging," J. Opt. Soc. Am. B **34**, B64–B77 (2017).
5. Y. Park, C. Depeursinge, and G. Popescu, "Quantitative phase imaging in biomedicine," Nat. Photonics **12**, 578–589 (2018).
6. E. Wolf, "Three-dimensional structure determination of semi-transparent objects from holographic data," Opt. Commun. **1**, 153 – 156 (1969).
7. J. Bailleul, B. Simon, M. Debailleul, L. Foucault, N. Verrier, and O. Haeberlé, "Tomographic diffractive microscopy: Towards high-resolution 3-d real-time data acquisition, image reconstruction and display of unlabeled samples," Opt. Commun. **422**, 28–37 (2018).
8. Y.-C. Lin and C.-J. Cheng, "Sectional imaging of spatially refractive index distribution using coaxial rotation digital holographic microtomography," J. Opt. **16**, 065401 (2014).
9. A. Kuś, M. Dudek, B. Kemper, M. Kujawińska, and A. Vollmer, "Tomographic phase microscopy of living three-dimensional cell cultures," J. biomedical optics **19**, 046009 (2014).
10. M. Habaza, B. Gilboa, Y. Roichman, and N. T. Shaked, "Tomographic phase microscopy with 180° rotation of live cells in suspension by holographic optical tweezers," Opt. Lett. **40**, 1881–1884 (2015).
11. Y. chih Lin, H.-C. Chen, H.-Y. Tu, C.-Y. Liu, and C.-J. Cheng, "Optically driven full-angle sample rotation for tomographic imaging in digital holographic microscopy," Opt. Lett. **42**, 1321–1324 (2017).
12. F. Merola, P. Memmolo, L. Miccio, R. Savoia, M. Mugnano, A. Fontana, G. D'Ippolito, A. Sardo, A. Iolascon, A. Gambale, and P. Ferraro, "Tomographic flow cytometry by digital holography," Light. Sci. &Amp; Appl. **6** (2017).
13. V. B., X.-J. Lai, Y.-C. Lin, H.-Y. Tu, and C.-J. Cheng, "Integrated dual-tomography for refractive index analysis of free-floating single living cell with isotropic superresolution," Sci. Reports **8** (2018).
14. B. Simon, M. Debailleul, M. Houkal, C. Ecoffet, J. Bailleul, J. Lambert, A. Spangenberg, H. Liu, O. Soppera, and O. Haeberlé, "Tomographic diffractive microscopy with isotropic resolution," Optica **4**, 460–463 (2017).
15. V. Lauer, "New approach to optical diffraction tomography yielding a vector equation of diffraction tomography and a novel tomographic microscope," J. Microsc. **205**, 165–176 (2002).
16. W. Choi, C. Fang-Yen, K. Badizadegan, S. Oh, N. Lue, R. R. Dasari, and M. S. Feld, "Tomographic phase microscopy," Nat. methods **4**, 717 (2007).
17. R. Fiolka, K. Wicker, R. Heintzmann, and A. Stemmer, "Simplified approach to diffraction tomography in optical microscopy," Opt. express **17**, 12407–12417 (2009).
18. M. Kim, Y. Choi, C. Fang-Yen, Y. Sung, R. R. Dasari, M. S. Feld, and W. Choi, "High-speed synthetic aperture microscopy for live cell imaging," Opt. letters **36**, 148–150 (2011).
19. S. O. Isikman, W. Bishara, S. Mavandadi, W. Y. Frank, S. Feng, R. Lau, and A. Ozcan, "Lens-free optical tomographic microscope with a large imaging volume on a chip," Proc. Natl. Acad. Sci. **108**, 7296–7301 (2011).
20. Y. Kim, H. Shim, K. Kim, H. Park, J. H. Heo, J. Yoon, C. Choi, S. Jang, and Y. Park, "Common-path diffraction optical tomography for investigation of three-dimensional structures and dynamics of biological cells," Opt. express **22**, 10398–10407 (2014).
21. P. Bon, S. Aknoun, S. Monneret, and B. Wattellier, "Enhanced 3d spatial resolution in quantitative phase microscopy using spatially incoherent illumination," Opt. express **22**, 8654–8671 (2014).
22. S. Shin, K. Kim, J. Yoon, and Y. Park, "Active illumination using a digital micromirror device for quantitative phase imaging," Opt. letters **40**, 5407–5410 (2015).
23. F. Momey, A. Berdeu, T. Bordy, J.-M. Dinten, F. K. Marcel, N. Picollet-D'Hahan, X. Gidrol, and C. Allier, "Lensfree diffractive tomography for the imaging of 3d cell cultures," Biomed. optics express **7**, 949–962 (2016).
24. L. Foucault, N. Verrier, M. Debailleul, B. Simon, and O. Haeberlé, "Simplified tomographic diffractive microscopy for axisymmetric samples," OSA Continuum **2**, 1039–1055 (2019).
25. E. Mudry, P. C. Chaumet, K. Belkebir, G. Maire, and A. Sentenac, "Mirror-assisted tomographic diffractive microscopy with isotropic resolution," Opt. Lett. **35**, 1857–1859 (2010).
26. Y. Park, M. Diez-Silva, G. Popescu, G. Lykotrafitis, W. Choi, M. S. Feld, and S. Suresh, "Refractive index maps and membrane dynamics of human red blood cells parasitized by plasmodium falciparum," Proc. Natl. Acad. Sci. **105**, 13730–13735 (2008).
27. Y. Sung, W. Choi, N. Lue, R. R. Dasari, and Z. Yaqoob, "Stain-free quantification of chromosomes in live cells using regularized tomographic phase microscopy," PloS one **7**, e49502 (2012).
28. J.-W. Su, W.-C. Hsu, C.-Y. Chou, C.-H. Chang, and K.-B. Sung, "Digital holographic microtomography for high-resolution refractive index mapping of live cells," J. biophotonics **6**, 416–424 (2013).
29. K. Kim, H. Yoon, M. Diez-Silva, M. Dao, R. R. Dasari, and Y. Park, "High-resolution three-dimensional imaging of red blood cells parasitized by plasmodium falciparum and in situ hemozoin crystals using optical diffraction tomography," J. biomedical optics **19**, 011005 (2013).

30. J. Yoon, K. Kim, H. Park, C. Choi, S. Jang, and Y. Park, "Label-free characterization of white blood cells by measuring 3d refractive index maps," Biomed. Opt. Express **6**, 3865–3875 (2015).
31. S. Lee, K. Kim, Y. Lee, S. Park, H. Shin, J. Ko, H. Park, and Y. Park, "Measurements of morphology and refractive indexes on human downy hairs using three-dimensional quantitative phase imaging," J. Biomed. Opt. **20**, 111207 (2015).
32. K. Kim, S. Lee, J. Yoon, J. Heo, C. Choi, and Y. Park, "Three-dimensional label-free imaging and quantification of lipid droplets in live hepatocytes," Sci. Reports **6** (2016).
33. J. Gatfield, K. Menyhart, D. Wanner, C. Gnerre, L. Monnier, K. Morrison, P. Hess, M. Iglarz, M. Clozel, and O. Nayler, "Selexipag active metabolite act-333679 displays strong anticontractile and antiremodeling effects but low $\beta$-arrestin recruitment and desensitization potential," J. Pharmacol. Exp. Ther. **362**, 186–199 (2017).
34. S. Chowdhury, W. J. Eldridge, A. Wax, and J. Izatt, "Refractive index tomography with structured illumination," Optica **4**, 537–545 (2017).
35. J. Jung, S.-J. Hong, H.-B. Kim, G. Kim, M. Lee, S. Shin, S. Lee, D.-J. Kim, C.-G. Lee, and Y. Park, "Label-free non-invasive quantitative measurement of lipid contents in individual microalgal cells using refractive index tomography," Sci. Reports **8** (2018).
36. A. Yakimovich, R. Witte, V. Andriasyan, F. Georgi, and U. F. Greber, "Label-free digital holo-tomographic microscopy reveals virus-induced cytopathic effects in live cells," mSphere **3** (2018).
37. A. Zamyadi, C. Romanis, T. Mills, B. Neilan, F. Choo, L. A. Coral, D. Gale, G. Newcombe, N. Crosbie, R. Stuetz, and R. K. Henderson, "Diagnosing water treatment critical control points for cyanobacterial removal: Exploring benefits of combined microscopy, next-generation sequencing, and cell integrity methods," Water Res. **152**, 96 – 105 (2019).
38. N. Streibl, "Three-dimensional imaging by a microscope," J. Opt. Soc. Am. A **2**, 121–127 (1985).
39. T. C. Wedberg and W. C. Wedberg, "Tomographic reconstruction of the cross-sectional refractive index distribution in semi-transparent, birefringent fibres," J. Microsc. **177**, 53–67 (1995).
40. M. Debailleul, B. Simon, V. Georges, O. Haeberlé, and V. Lauer, "Holographic microscopy and diffractive microtomography of transparent samples," Meas. Sci. Technol. **19**, 074009 (2008).
41. B. Simon, M. Debailleul, A. Beghin, Y. Tourneur, and O. Haeberlé, "High-resolution tomographic diffractive microscopy of biological samples," J. Biophotonics **3**, 462–467 (2010).
42. K. Kim, H. Yoon, M. Diez-Silva, M. Dao, R. R. Dasari, and Y. Park, "High-resolution three-dimensional imaging of red blood cells parasitized by *Plasmodium falciparum* and *in situ* hemozoin crystals using optical diffraction tomography," J. Biomed. Opt. **19**, 011005 (2013).
43. https://nanolive.ch/.
44. http://tomocube.com/.
45. S. A. Alexandrov, T. R. Hillman, T. Gutzler, and D. D. Sampson, "Synthetic aperture fourier holographic optical microscopy," Phys. review letters **97**, 168102 (2006).
46. V. Mico, Z. Zalevsky, P. García-Martínez, and J. García, "Synthetic aperture superresolution with multiple off-axis holograms," JOSA A **23**, 3162–3170 (2006).
47. J. R. Price, P. R. Bingham, and C. E. Thomas Jr, "Improving resolution in microscopic holography by computationally fusing multiple, obliquely illuminated object waves in the fourier domain," Appl. optics **46**, 827–833 (2007).
48. J. Bühl, H. Babovsky, A. Kiessling, and R. Kowarschik, "Digital synthesis of multiple off-axis holograms with overlapping fourier spectra," Opt. Commun. **283**, 3631–3638 (2010).
49. M. Sarmis, B. Simon, M. Debailleul, B. Colicchio, V. Georges, J.-J. Delaunay, and O. Haeberle, "High resolution reflection tomographic diffractive microscopy," J. Mod. Opt. **57**, 740–745 (2010).
50. H. Liu, J. Bailleul, B. Simon, M. Debailleul, B. Colicchio, and O. Haeberlé, "Tomographic diffractive microscopy and multiview profilometry with flexible aberration correction," Appl. optics **53**, 748–755 (2014).
51. G. Maire, Y. Ruan, T. Zhang, P. C. Chaumet, H. Giovannini, D. Sentenac, A. Talneau, K. Belkebir, and A. Sentenac, "High-resolution tomographic diffractive microscopy in reflection configuration," JOSA A **30**, 2133–2139 (2013).
52. S. Vertu, J.-J. Delaunay, I. Yamada, and O. Haeberlé, "Diffraction microtomography with sample rotation: influence of a missing apple core in the recorded frequency space," Cent. Eur. J. Phys. **7**, 22–31 (2009).
53. S. Vertu, J. Flügge, J.-J. Delaunay, and O. Haeberlé, "Improved and isotropic resolution in tomographic diffractive microscopy combining sample and illumination rotation," Cent. Eur. J. Phys. **9**, 969–974 (2011).
54. S. Hell and E. H. K. Stelzer, "Properties of a 4pi confocal fluorescence microscope," J. Opt. Soc. Am. A **9**, 2159–2166 (1992).
55. A. Bilenca, J. Cao, M. Colice, A. Ozcan, B. Bouma, L. Raftery, and G. Tearney, "Fluorescence interferometry," Annals New York Acad. Sci. **1130**, 68–77 (2008).
56. M. Born and E. Wolf, *Principles of optics: electromagnetic theory of propagation, interference and diffraction of light* (Elsevier, 2013).
57. https://omlc.org/calc/mie_calc.html.
58. C. Park, S. Shin, and Y. Park, "Generalized quantification of three-dimensional resolution in optical diffraction tomography using the projection of maximal spatial bandwidths," JOSA A **35**, 1891–1898 (2018).
59. C. Godavarthi, T. Zhang, G. Maire, P. C. Chaumet, H. Giovannini, A. Talneau, K. Belkebir, and A. Sentenac, "Superresolution with full-polarized tomographic diffractive microscopy," JOSA A **32**, 287–292 (2015).